Hindawi
Mathematical Problems in Engineering
Volume 2022, Article ID 7408232, 13 pages
https://doi.org/10.1155/2022/7408232

Research Article

A Closure Jacking Force Calculation Algorithm for Curved Prestressed Concrete Continuous Rigid-Frame Bridges with Asymmetric Cantilevers and Piers

Chuang Chen,[1] **Xuyi Wang**,[2] **Qidong Lin**,[3] **and Yinhui Wang**[1]

[1]*School of Civil and Architectural Engineering, Ningbo Tech University, Ningbo, China*
[2]*Zhejiang Scientific Research Institute of Transportation, Hangzhou, China*
[3]*Ningbo Communication Construction Engineering Testing Center Co., Ltd, Ningbo, China*

Correspondence should be addressed to Yinhui Wang; wangyh7244@nit.zju.edu.cn

Received 29 January 2022; Accepted 18 May 2022; Published 31 May 2022

Academic Editor: Francesco Foti

Concrete continuous rigid-frame bridges are the most commonly used to cross exciting highway and railway. Before the bridge closure, the closure jacking force (CJF) needs to be determined firstly, which plays an important role in mid-span deflection controlling and the whole bridge stress state. This study proposed a closure jacking force calculation algorithm for curved prestressed concrete continuous rigid-frame bridges with asymmetric cantilevers and piers. Firstly, the mechanics method was used to analyze the relationship between the CJF and normal stress of main-girder and the pier. In addition, an actual bridge was taken as a numerical simulation case to determine the influence of the deformation and the stress induced by concrete shrinkage and creep of the main-girder and the jacking force. Finally, in order to obtain the optimal stress state of bridge piers, the multi-objective linear programming method was proposed to calculate the CJF. The results show that curved prestressed concrete continuous rigid-frame bridges usually suffered longitudinal and transverse bending and torsion under the concrete shrinkage and creep of the main-girder and the CJF, and the CJF significantly affected the normal stress of the pier with a low anti-push rigidity. The normal stress of piers was obviously linear with the CJF during whole construction and operation state of bridges at the following three states: the jacking process, bridge completion, and ten years of bridge operation. The multi-objective linear programming algorithm was an effective way to determine the optimal CJF and can fully reflect both longitudinal and transverse bending of piers.

1. Introduction

Newly bridges crossing existing routes, valleys, and other complex terrain conditions have to meet the challenge in the structural form. The prestressed concrete continuous rigid-frame (PCCR) bridge considered as the most competitive potential bridge form can provide great spanning ability and mature construction technology for wide application. Sometimes, PCCR bridges need to overcome difficulties such as long span, asymmetrical cantilever, curved girder with small curvature radius, and swivel girder. Generally, the main-girder needs to keep on full-section compression under the action of dead load. After bridge completion, the main-girder will contract with time because of temperature decreasing and concrete shrinkage and creep [1]. For curved PCCR bridges, the expansion and contraction of the main-girder will force the pier suffer longitudinal transverse and torsional deformation. More seriously, these expansion and contraction even can lead concrete crack at the pier-bottom, so as to affect the safety and durability of bridges. Therefore, before the closure of curved PCCR bridges, the main-girder usually needs to be pushed from the middle for decreasing the longitudinal, transverse, and torsional deformation of piers [2, 3].

At present, previous studies mainly focused on closure jacking force (CJF) controlling methods and calculation theories for different types of bridges, such as three-span and multi-span continuous rigid-frame bridges [4, 5], V-shaped

pier continuous rigid-frame bridges [6], asymmetric continuous rigid-frame bridges [7], truss-type steel-pipe concrete arch bridges [8], and extra-dosed cable-stayed bridges [9]. However, there are rare theoretical studies on CJF algorithms for curved continuous rigid-frame bridges, especially with asymmetric cantilever and piers. The CJF of small-radius curved PCCR bridges with asymmetric cantilever is hard for determining Because that two-dimensional asymmetry piers will lead the jacking stiffness different providing for the CJF [10]. In addition, these piers will suffer on sustained stress coupling with bending, shear, and torsion deformation during the jacking construction process. At last, the curvature main-girder may also suffer lateral bending additionally during the jacking construction process. For above reasons, it is essential to conduct an in-depth study on the closure jacking control theory for curved PCCR bridges with an asymmetric cantilever and piers.

The core of the closure jacking controlling is to determine the closure jacking force and the closure jacking displacement. The CJF can be determined by the pier-top deformation induced by ten years of shrinkage and creep and the closure temperature difference of the main-girder [11–13]. The results show that closure jacking controlling can effectively improve the stress state of piers and main-girder's deflection. Besides, in order to avoid excessive longitudinal displacement at pier-top after bridge completion, Sun and Zhao [14] determined the closure jacking displacement by the half longitudinal displacement of the pier-top induced by closure temperature difference and the 10th year concrete shrinkage and creep of main-girder. Wen [15] took half displacement of the pier-top induced by the 30th year concrete shrinkage and creep of auxiliary bridge of Sutong Bridge as the closure jacking displacement. Zhang and Wu [16] determined the upper and lower limits of the CJF according to pier crack and main-girder stress, and took the counteracted displacement at pier-top caused by three years of main-girder concrete shrinkage and creep as the jacking displacement. Liang [17] determined the CJF according to the combination of the pier-top displacement after bridge completion, 70% pier-top displacement induced by main-girder concrete shrinkage and creep, and the pier-top displacement induced by closure temperature difference. Thus, there are no unified standards and theoretical basis of the calculation methodology of the CJF and the jacking displacement for PCCR bridges.

In this study, a closure jacking force calculation algorithm for curved prestressed concrete continuous rigid-frame bridges with asymmetric cantilevers and piers was proposed. Firstly, a mechanical relation between the normal stress and the jacking force of the pier of curved PCCR bridges was derived, and the influence of the jacking force on the stress state of the main-girder and the pier was analyzed. The multi-objective linear programming method was used to determine the jacking force, and the calculation process was given. In addition, a real long-span curved PCCR bridge with asymmetric cantilevers and piers was simulated for indicating the influence of concrete shrinkage and creep of the main-girder and the jacking force on the deformation and stress of piers. Finally, taking the optimal stress states (the time of bridge completion, ten years of bridge operation, and both) of piers as objectives, a CJF calculation algorithm was proposed for looking for the optimal jacking force based on the multi-objective linear programming method.

2. Theoretical Analysis of the Closure Jacking Force

2.1. Mechanical Analysis of Jacking Construction of Curved Continuous Rigid-Frame Bridges. Curved continuous rigid-frame bridges bear the closure jacking force under the maximum single cantilever state. Not only it is subjected to concentrated load F along the tangential direction, but also an eccentric bending moment $F{\cdot}e$ is generated due to the deviation of the jacking force from the section centroid [2], where e is the vertical deviation distance. A mechanics model is shown in Figure 1. In a general case, the bridge satisfies that each dimension of the cross section is far less than the span length dimension. The shear center of each section is coinciding with the centroid, and the calculation satisfies the plane cross-sectional assumption and the rigid cross-sectional assumption [18]. Therefore, main-girder and piers stress can be solved by the force method in the maximum single cantilever state with the action of the jacking force. The curved continuous rigid-frame bridge with the maximum single cantilever can be considered as the quadratic statically indeterminate structure. The excess unknown forces X_1 and X_2 are used to replace the vertical support constraint and horizontal radial constraint of supports. The basic mechanical model is shown in Figure 2.

The curved beam radius is R. Its central angle corresponding to cantilever mid-span length is θ_1, and to cantilever side span is θ_2. The pier and the main-girder are both assumed as uniform cross section. Their elasticity modulus is E_p and E_b, and shear modulus is G_p and G_b. Their equivalent polar moment of inertia is I_{tp} and I_{tb}, respectively. The inertia moments of the main-girder around axis y and axis z of the local coordinate system are I_{by} and I_{bz}, and those of the pier are I_{py} and I_{pz}, respectively.

The basic mechanical model should have no vertical displacement under the redundant unknown force. The force method equations can be written as follows:

$$\begin{cases} \delta_{11}X_1 + \delta_{12}X_2 + \Delta_{1P} = 0, \\ \\ \delta_{21}X_1 + \delta_{22}X_2 + \Delta_{2P} = 0. \end{cases} \tag{1}$$

When $0 \le \alpha \le \theta_1$, the beam internal force is

$$\begin{aligned} M_{\mathrm{bz}} &= -\mathrm{FR}(1 - \cos\alpha), \\ M_{\mathrm{by}} &= \mathrm{Fe}\cos\alpha, \\ T_b &= M_{\mathrm{bx}}, \\ &= -\mathrm{Fe}\sin\alpha. \end{aligned} \tag{2}$$

The pier internal force $(0 \le h \le l)$ is

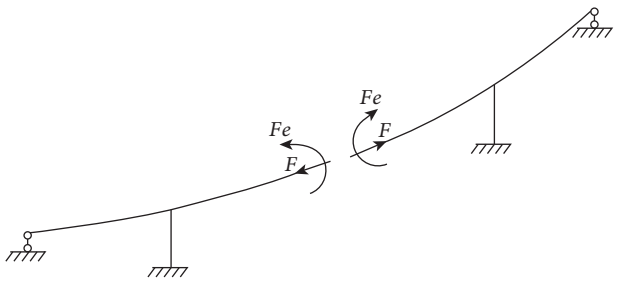

Figure 1: Mechanics model of a three-span curved continuous beam during closure jacking process.

$$\begin{aligned} M_{\mathrm{py}} &= \mathrm{Fh}\cos\theta_1 + \mathrm{Fe}\cos\theta_1 \\ &= aF, \\ M_{\mathrm{pz}} &= \mathrm{Fh}\sin\theta_1 + \mathrm{Fe}\sin\theta_1 \\ &= bF, \\ T_{\mathrm{p}} &= M_{\mathrm{px}} \\ &= -\mathrm{FR}(1-\cos\theta_1), \end{aligned} \tag{3}$$

where $a = h\cos\theta_1 + e\cos\theta_1$ and $b = h\sin\theta_1 + e\sin\theta_1$.

When a unit unknown force $X_1 = 1$ acts on the basic structure and $\theta_1 \le \alpha \le \theta_1 + \theta_2$, the beam internal force is

$$\begin{aligned} \overline{M}_{\mathrm{by1}} &= -R\sin(\theta_1 + \theta_2 - \alpha), \\ \overline{T}_{b1} &= \overline{M}_{\mathrm{bx1}} \\ &= -R\cdot[1-\cos(\theta_1+\theta_2-\alpha)]. \end{aligned} \tag{4}$$

The pier internal force $(0 \le h \le l)$ is

$$\begin{aligned} \overline{M}_{\mathrm{py1}} &= -R\sin\theta_2, \\ \overline{M}_{\mathrm{pz1}} &= R(1-\cos\theta_2). \end{aligned} \tag{5}$$

When a unit unknown force $X_2 = 1$ acts on the basic structure and $\theta_1 \le \alpha \le \theta_1 + \theta_2$, the beam internal force is

$$\overline{M}_{\mathrm{bz2}} = R\sin(\theta_1 + \theta_2 - \alpha). \tag{6}$$

The pier internal force $(0 \le h \le l)$ is

$$\begin{aligned} \overline{M}_{\mathrm{py2}} &= h\sin\theta_2, \\ \overline{M}_{\mathrm{pz2}} &= h\cos\theta_2, \\ \overline{T}_{\mathrm{p2}} &= M_{\mathrm{px2}}, \\ &= R\sin\theta_2. \end{aligned} \tag{7}$$

The shear force and the axial force can be neglected when calculating curved beam deflection. However, the bending moment and the torsional moment need to be involved [18]. According to Vlasov differential equation [19], the beam vertical displacement has no association with the bending moment M_z, so the following equations can be obtained:

$$\begin{aligned} \delta_{11} &= \sum\int \frac{\overline{M}^2}{\mathrm{EI}}\mathrm{d}s + \sum\int \frac{\overline{T}^2}{\mathrm{GI}_t}\mathrm{d}s, \\ &= \int_{\theta_1}^{\theta_1+\theta_2} \frac{\overline{M}_{\mathrm{by1}}{}^2}{E_{\mathrm{by}}I_{\mathrm{by}}} + \frac{\overline{T}_{b1}{}^2}{G_bI_{\mathrm{tb}}}\mathrm{d}\alpha + \int_0^l \frac{\overline{M}_{\mathrm{py1}}{}^2}{E_{\mathrm{py}}I_{\mathrm{py}}} + \frac{\overline{M}_{\mathrm{pz1}}{}^2}{E_{\mathrm{pz}}I_{\mathrm{pz}}}\mathrm{d}h, \\ &= \frac{lR^2\sin^2\theta_2}{E_{\mathrm{py}}I_{\mathrm{py}}} + \frac{R^3(2\theta_2 - \sin 2\theta_2)}{4E_{\mathrm{by}}I_{\mathrm{by}}}, \\ &\quad + \frac{R^2l(1-\cos\theta_2)^2}{E_{\mathrm{pz}}I_{\mathrm{pz}}} + \frac{R^3(6\theta_2 + \sin 2\theta_2 - 8\sin\theta_2)}{4G_bI_{\mathrm{tb}}}, \\ \delta_{12} &= \delta_{21}, \\ &= \sum\int \frac{\overline{M}^2}{\mathrm{EI}}\mathrm{d}s, \\ &= \int_0^l \frac{\overline{M}_{\mathrm{py1}}\overline{M}_{\mathrm{py2}}}{E_{\mathrm{py}}I_{\mathrm{py}}} + \frac{\overline{M}_{\mathrm{pz1}}\overline{M}_{\mathrm{pz2}}}{E_{\mathrm{pz}}I_{\mathrm{pz}}}\mathrm{d}h, \\ &= \frac{Rl^2(\cos\theta_2 - \cos^2\theta_2)}{2E_{\mathrm{pz}}I_{\mathrm{pz}}} - \frac{Rl^2\sin^2\theta_2}{2E_{\mathrm{py}}I_{\mathrm{py}}}, \\ \Delta_{1p} &= \sum\int \frac{\overline{M}M}{\mathrm{EI}}\mathrm{d}s, \\ &= \int_0^h \frac{\overline{M}_{\mathrm{py1}}M_{\mathrm{py}}}{E_{\mathrm{py}}I_{\mathrm{py}}} + \frac{\overline{M}_{\mathrm{pz1}}M_{\mathrm{pz}}}{E_{\mathrm{pz}}I_{\mathrm{pz}}}\mathrm{d}h, \\ &= \left[\frac{(1-\cos\theta_2)\sin\theta_1}{2E_{\mathrm{pz}}I_{\mathrm{pz}}} - \frac{\sin\theta_2\cos\theta_1}{2E_{\mathrm{py}}I_{\mathrm{py}}}\right]\mathrm{FRl}(l+2e), \\ &= cF, \\ \delta_{22} &= \sum\int \frac{\overline{M}^2}{\mathrm{EI}}\mathrm{d}s + \sum\int \frac{\overline{T}^2}{\mathrm{GI}_t}\mathrm{d}s, \\ &= \int_{\theta_1}^{\theta_1+\theta_2} \frac{\overline{M}_{bz2}^2}{E_{\mathrm{bz}}I_{\mathrm{bz}}}\mathrm{d}\alpha + \int_0^l \frac{\overline{M}_{py2}^2}{E_{\mathrm{py}}I_{\mathrm{py}}} + \frac{\overline{M}_{pz2}^2}{E_{\mathrm{pz}}I_{\mathrm{pz}}}\mathrm{d}l + \int_0^l \frac{\overline{T}_{p2}{}^2}{G_pI_{\mathrm{tp}}}\mathrm{d}l, \\ &= \frac{R^3(2\theta_2 - \sin 2\theta_2)}{4E_{\mathrm{bz}}I_{\mathrm{bz}}} + \frac{l^3\sin^2\theta_2}{3E_{\mathrm{py}}I_{\mathrm{py}}}, \\ &\quad + \frac{l^3\cos^2\theta_2}{3E_{\mathrm{pz}}I_{\mathrm{pz}}} \\ \Delta_{2p} &= \sum\int \frac{\overline{M}_2M}{\mathrm{EI}}\mathrm{d}s + \sum\int \frac{\overline{T}_2T}{\mathrm{GI}_t}\mathrm{d}s, \\ &= \int_0^l \frac{\overline{M}_{\mathrm{py2}}M_{\mathrm{py}}}{E_{\mathrm{py}}I_{\mathrm{py}}} + \frac{\overline{M}_{\mathrm{pz2}}M_{\mathrm{pz}}}{E_{\mathrm{pz}}I_{\mathrm{pz}}} + \frac{\overline{T}_{p2}T_p}{G_pI_{\mathrm{tp}}}\mathrm{d}h, \\ &= \left(\frac{\cos\theta_1\sin\theta_2}{6E_{\mathrm{py}}I_{\mathrm{py}}} + \frac{\sin\theta_1\cos\theta_2}{6E_{\mathrm{pz}}I_{\mathrm{pz}}}\right)\mathrm{Fl}^2(3e+2l) \\ &\quad - \frac{\mathrm{FlR}\sin\theta_2(1-\cos\theta_1)}{G_pI_{\mathrm{tp}}} \\ &= \mathrm{d}F, \end{aligned} \tag{8}$$

where $c = [(1-\cos\theta_2)\sin\theta_1/2E_{\mathrm{pz}}I_{\mathrm{pz}} - \sin\theta_2\cos\theta_1/2E_{\mathrm{py}}I_{\mathrm{py}}]\mathrm{Rl}(l+2e)$ and $\mathrm{d} = (\cos\theta_1\sin\theta_2/6E_{\mathrm{py}}I_{\mathrm{py}} +$

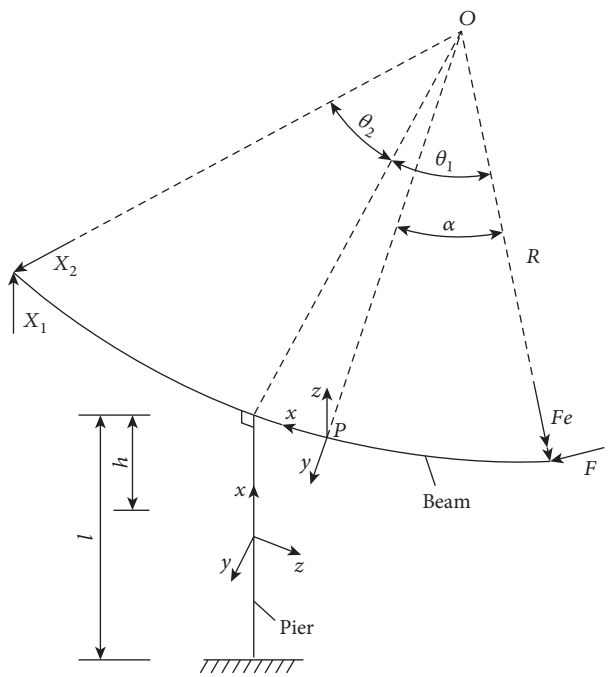

Figure 2: Basic mechanical model.

$\sin\theta_1 \cos\theta_2/6E_{pz}I_{pz})l^2(3e+2l) - lR\sin\theta_2(1-\cos\theta_1)/G_pI_{tp}$.

According to the Force (1), the following equations can be obtained:

$$\begin{cases} X_1 = \dfrac{\delta_{12}\Delta_{2P} - \delta_{22}\Delta_{1P}}{\delta_{11}\delta_{22} - \delta_{12}\delta_{21}} \\ = mF, \\ X_2 = \dfrac{\delta_{11}\Delta_{2P} - \delta_{21}\Delta_{1P}}{\delta_{12}\delta_{21} - \delta_{11}\delta_{22}} \\ = nF, \end{cases} \tag{9}$$

where $m = \delta_{12}d - \delta_{22}c/\delta_{11}\delta_{22} - \delta_{12}\delta_{21}$ and $n = \delta_{11}d - \delta_{21}c/\delta_{12}\delta_{21} - \delta_{11}\delta_{22}$.

Thus, the beam internal force under jacking force can be obtained as follows:

When $0 \le \alpha \le \theta_1$,

$$\begin{aligned} M_{bz} &= -\mathrm{FR}(1-\cos\alpha), \\ M_{by} &= Fe\cos\alpha, \\ T_b &= M_{bx} \\ &= -Fe\sin\alpha. \end{aligned} \tag{10}$$

When $\theta_1 \le \alpha \le \theta_1 + \theta_2$,

$$\begin{aligned} M_{\mathrm{by}} &= -m\mathrm{FR}\sin(\theta_1+\theta_2-\alpha), \\ T_{\mathrm{b}} &= M_{\mathrm{bx}}, \\ &= -m\mathrm{FR}[1-\cos(\theta_1+\theta_2-\alpha)] \\ M_{\mathrm{bz}} &= n\mathrm{FR}\sin(\theta_1+\theta_2-\alpha). \end{aligned} \tag{11}$$

When $0 \le h \le l$, the internal force of the bridge pier is

$$\begin{aligned} M_{\mathrm{py}} &= aF - m\mathrm{FR}\sin\theta_2 + n\mathrm{Fh}\sin\theta_2, \\ M_{\mathrm{pz}} &= \mathrm{bF} + m\mathrm{FR}(1-\cos\theta_2) + n\mathrm{Fh}\cos\theta_2, \\ T_p &= -\mathrm{FR}(1-\cos\theta_1) + n\mathrm{FR}\sin\theta_2. \end{aligned} \tag{12}$$

Thus, the vertical normal stress of any point (x, y, z) on the pier can be further calculated as follows:

$$\begin{aligned} \sigma_{\mathrm{px}} &= \frac{\sum M_y}{I_y}z + \frac{\sum M_z}{I_z}y, \\ &= \frac{M_{\mathrm{py}} + \overline{M}_{\mathrm{py1}}X_1 + \overline{M}_{\mathrm{py2}}X_2}{I_{\mathrm{py}}}z + \frac{M_{\mathrm{pz}} + \overline{M}_{\mathrm{pz1}}X_1 + \overline{M}_{\mathrm{pz2}}X_2}{I_{\mathrm{pz}}}y \\ &= kF, \end{aligned} \tag{13}$$

where $k = a + m\overline{M}_{\mathrm{py1}} + n\overline{M}_{\mathrm{py2}}g/I_{\mathrm{py}}z + b + m\overline{M}_{\mathrm{pz1}}e + n\overline{M}_{\mathrm{pz2}}/I_{\mathrm{pz}}y$

Above all, it can be observed that c, d, m, and n are always constants. For a certain section of the main-girder and piers (a or h is also the constant), the coefficients a and b are constant. The bending moment and the torque of any section of the main-girder and piers are directly proportional to the jacking force. It can be known from (13), for a certain point (x_0, y_0, z_0) at the pier, coefficient k is a constant, so the vertical normal stress at this point presents linear relationship with the jacking force, too. Moreover, the jacking force not only forces the pier to suffer longitudinal bending, but also causes the pier to suffer lateral bending and torsion bending, and it is mainly affected by the height of the pier, the radius of the curved beam, and the cantilever length of the curved beam. In this point, the jacking force makes the pier in the stress state coupling with bending, shear, and torsion under the maximum single cantilever condition of the main beam. Therefore, the CJF can effectually improve the pier's longitudinal bending, transverse bending, and torsional deformation at the same time. It should be noted that the jacking force can also make the beam produce transverse bending and torsional deformation, and it is mainly affected by the radius of the curved beam, the cantilever length of the curved beam, and the distance between the jacking force and the centroid of the section.

2.2. Closure Jacking Force Algorithm Based on the Multi-Objective Linear Programming Method. The proper closure jacking force can make the pier in optimal stress state and make each section of the pier keep minimum tensile stress after bridge completion. Based on above derivation, it can be observed that the pier's vertical normal stress and the jacking force show a linear relationship during the closure jacking process, and the jacking force calculation issue can be solved by constrained multi-objective linear programming method [9, 20]. Then, linear expression equations for the jacking force can be written as follows:

$$\sigma_{dj} = \sum_{1 \le i \le r} \alpha_{ji} x_i + \sum \sigma_{jc} \le [\sigma], \tag{14}$$

where σ_{dj} is the stress of the j-th pier after the central span closure jacking; x_i is the CJF at i-th position; α_{ji} is the stress variation of the i-th position of the j-th pier under the unit jacking force; σ_{jc} is the stress of the j-th pier under the construction load; and $[\sigma]$ is the allowable tensile stress of the pier.

Without considering the effect of the jacking force on concrete creep, a linear relationship between the vertical normal stress of the j-th pier and the jacking force at one time point after bridge completion can be established as follows:

$$\sigma_{cj} = \sum_{1 \le i \le r} \beta_{ji} x_i + \sum \sigma_{jg} + \sum \sigma_{jq}, \tag{15}$$

where σ_{cj} is the stress of the j-th pier at one time point after bridge completion; x_i is the jacking force at the i-th position; β_{ji} is the stress variation of the i-th position of the j-th pier at one time point after bridge completion under the unit jacking force; $\sum \sigma_{jg}$ is the stress of the j-th pier under the dead load; and $\sum \sigma_{jq}$ is the stress of the j-th pier under the live load.

Notably, if the jacking force changes concrete creep secondary interior force, the pier stress is not completely in a linear correlation with the jacking force, but the jacking force can be modified through iteration. Thus, the constrained multi-objective achieving problem in solving the jacking force can be solved using the multi-objective linear programming method, and the optimal jacking force can be calculated according to the following procedure:

(1) The control section of pier and the pier allowable stress $[\sigma]$ in the construction stage is determined according to relevant specifications or concrete material performance tests.

(2) The parameter $\sigma_{\alpha j0}$和$\sigma_{\beta j0}$ can be calculated based on the numerical simulation model of the bridge, and the stress of j-th pier during the jacking process and at a time point in the bridge operational state under the action of no jacking force is denoted.

(3) The initial jacking force x_{i1} is set to calculate $\sigma_{\alpha ji1}$ and $\sigma_{\beta ji1}$, and the stress changes of j-th pier during the jacking process and at a time point in the bridge operational state under the action of jacking force x_{i1} at i-th position are denoted. Then, $\Delta\sigma_{\alpha ji1} = \sigma_{\alpha ji1} - \sigma_{\alpha j0}$ and $\Delta\sigma_{\beta ji1} = \sigma_{\beta ji1} - \sigma_{\beta j0}$ can be obtained.

(4) The linear change rates $\alpha_{ji1} = \Delta\sigma_{\alpha ji1}/x_{i1}$ and $\beta_{ji1} = \Delta\sigma_{\beta ji1}/x_{i1}$ of stress are calculated.

(5) Formula (14) is taken as constraint condition, and formula (15) is taken as objective function. Therefore, the jacking force x_{i2} due to constrained multi-objective linear programming method function of MATLAB can be obtained.

(6) The jacking force x_{i2} is applied to the structure, and then Procedures (3)–(5) are repeated. After several iterations, when the relative error of the jacking force calculated in the previous and last two calculations meets the expectation, the calculation can stop and the optimal jacking force can be obtained.

It can be seen that the constrained multi-objective linear programming method has the following advantages:

(1) The control objectives are clear, such as the optimal force of the bridge pier in the state of the bridge.

(2) The method can make multiple bridge piers (the stress state including multiple sections and multiple parts) simultaneously reach the optimal stress state, and can overcome the traditional method that can only control the bending effect of bridge piers in one direction.

(3) The concrete stress is prevented from exceeding the allowable value during the construction process.

(4) The solution process is practical and the solution is efficient due to the linear relationship between the normal stress of the bridge pier and the jacking force.

3. A Bridge Case Study

3.1. Bridge Background. In this study, a bridge in Ningbo city of China over crossing two paralleled railways was taken as a case study. This bridge is a prestressed concrete continuous rigid-frame bridge with large spans, small curvature radius, asymmetry cantilevers and piers, and swivel construction. The bridge has a total length 301 m, and the span arrangement is 68 + 138+95 m. The bridge curvature radius of the center upstream line is 350 m, and the main-girder top and bottom flanges are 11 m and 7 m wide, respectively. An asymmetric span arrangement is used for this bridge with the length of the two T-frame cantilevers 50 m and 86 m, respectively. The main-girder of T-frame (small T-frame) is 5–9 m in height (changing according to 1.8-degree parabola) with 13 segments through symmetric cast-in-place cantilever method. The main-girder of T-frame (large T-frame) is 5–12 m in height (changing according to the 1.8-degree parabola, too) with 22 segments. Box sections are used for the pier, and the two piers are asymmetric in height and cross section. Pier 27# is 17.65 m high, and the pier-top horizontal width is 7 m. The longitudinal length at pier-top and pier-bottom is both 5.5 m, and the pier-bottom lateral width is 8.6 m. Pier 28# is 16.55 m high. Its lateral width and the longitudinal length at pier-top are 7 m and 6.5 m, respectively. Its lateral width and longitudinal length at pier-bottom are 11.4 m and 6.5 m, respectively. The bridge elevation view is shown in Figure 3. The view before and after girder rotation is shown in Figure 4. The side views of two piers are shown in Figure 5. The bridge site construction view is shown in Figure 6.

3.2. Finite Element Model. The finite element software MIDAS/civil was used to establish the calculation model of the bridge as shown in Figure 7. The finite element model had 881 units and 918 nodes in total. The vertical ordinary reinforcements of the pier were established, and their effect was considered in calculating the pier stiffness. The main-

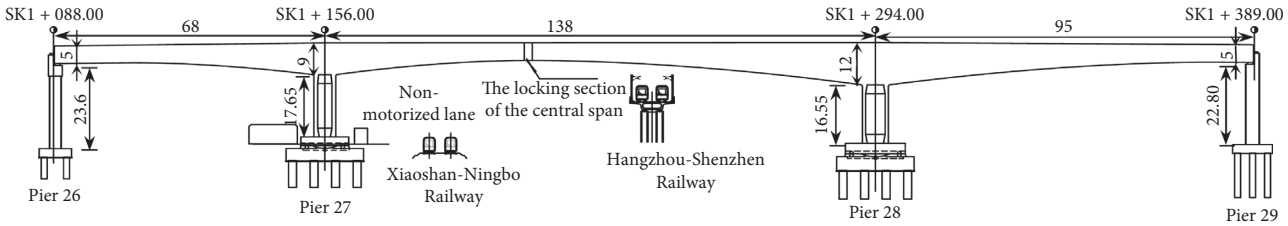

Figure 3: Bridge elevation view (unit: (m)).

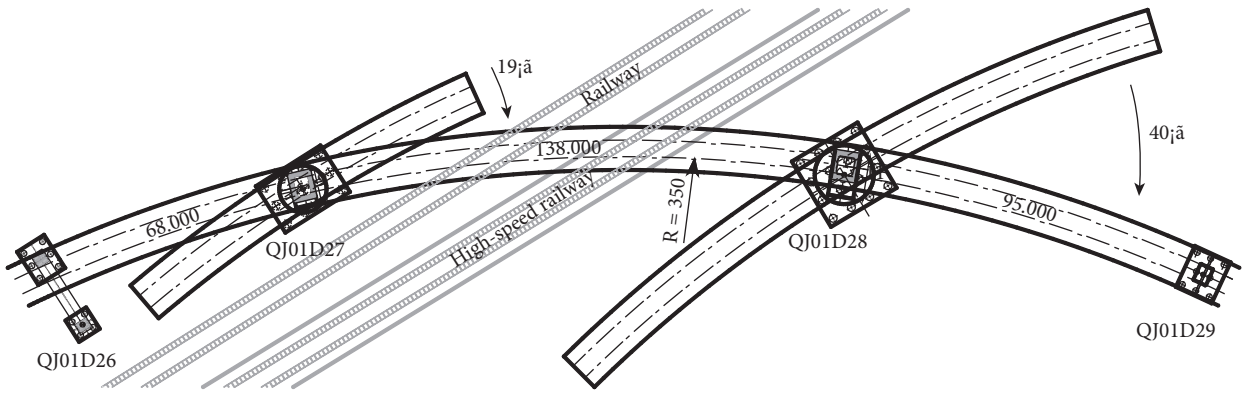

Figure 4: The view before and after girder rotation (unit: (m)).

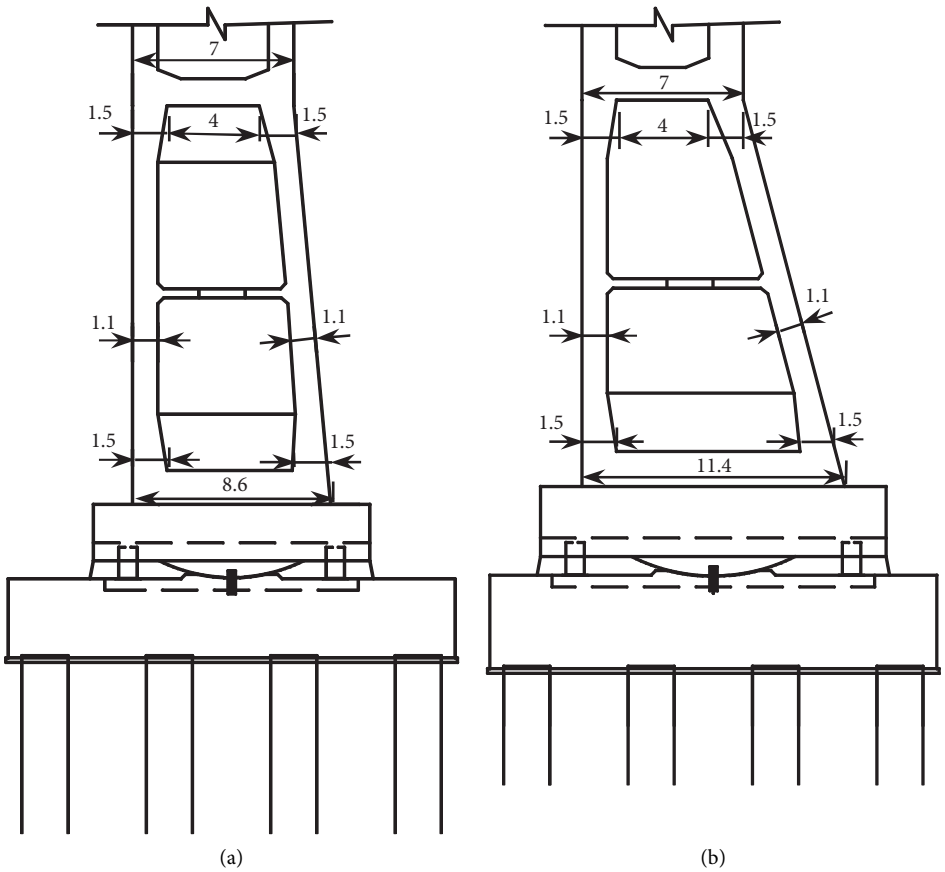

Figure 5: Side view of piers (unit: (m)): (a) side view for Pier 27#; (b) side view for Pier 28#.

Figure 6: Bridge site on construction.

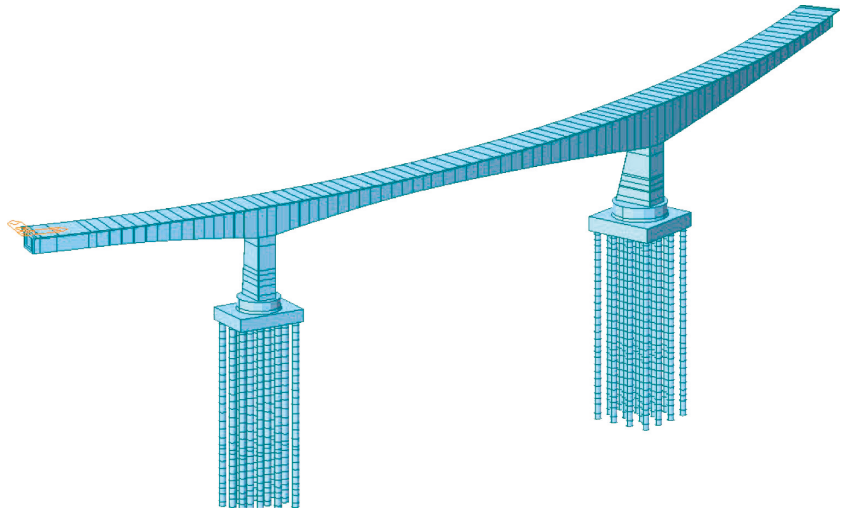

Figure 7: Finite element model.

girder, piers, cushion caps, and pile foundations were connected by the elastic-rigid connections. The pile-bottom was restrained by the consolidation. Regarding pile-soil interaction, the "m" method was used to calculate the soil spring stiffness of each soil layer, which was taken as the boundary condition and directly applied to the nodes of piles. Both sides at the girder end were restrained according to the actual support conditions, and the longitudinal movable bearing and bidirectional movable bearing were simulated, where the bidirectional movable bearing only simulated the vertical support with the value for vertical stiffness taken as 5×106 kN/m. The longitudinal movable bearing constrained the vertical displacement and the radial displacement. Totally, 90 construction stages in the model were established according to actual construction processes, and the cantilever construction of each section was divided into three construction stages: hanging basket installation, concrete construction, and prestressed tension. A dead-load torque of the curved girder was applied through node torque.

4. Results and Analysis

4.1. Main-Girder Concrete Shrinkage and Creep-Induced Pier Deformation. Concrete shrinkage and creep make the main-girder shorten and force the pier suffer longitudinal deformation, which is the most important reason why the closure jacking is necessary. During the bridge operation, the pier-top deformation of Pier 27# and Pier 28# induced by concrete shrinkage and creep of main-girder is shown in Figure 8, where x is the displacement, θ is the angle, and a is the time. For longitudinal displacement, a smaller pile number's pointing to a greater pile number is taken as "+"; for lateral displacement, radially pointing to the center of circle along the curve is taken as "+"; for torsion angle, the counterclockwise rotation is taken as "+."

From Figure 8, it can be noticed that main-girder concrete shrinkage and creep can force Pier 27# and Pier 28# clockwise and counterclockwise rotation, respectively. Specifically, the pier-top longitudinal displacement and torsion angle of Pier 27# will increase from 5.81 mm and 0.54×10^{-4} rad just after bridge completion to 16.95 mm and 2.29×10^{-4} rad in ten years of bridge operation, respectively, the lateral displacement will change from −0.07 mm to 4.43 mm. The pier-top longitudinal displacement and torsion angle of Pier 28# will increase from −4.15 mm and -0.74×10^{-4} rad just after bridge completion to −12.32 mm and -2.49×10^{-4} rad in ten years of bridge operation, respectively, and the lateral displacement transforms from

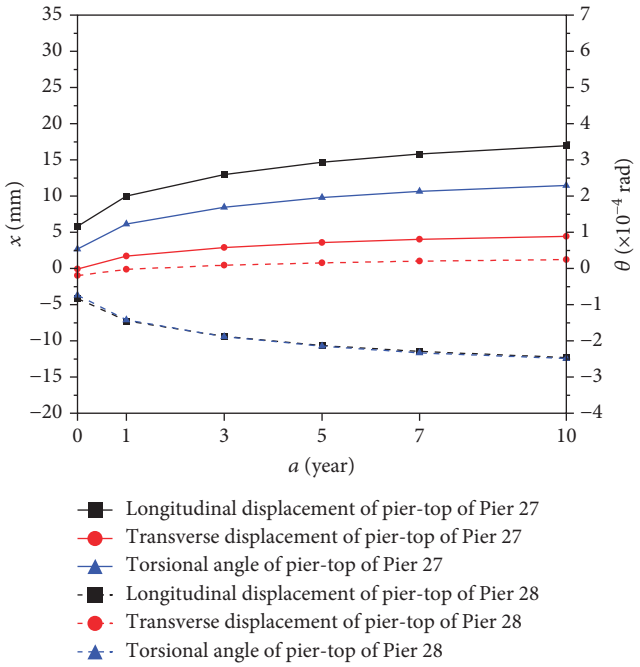

Figure 8: Main-girder concrete shrinkage and creep effect on pier deformation.

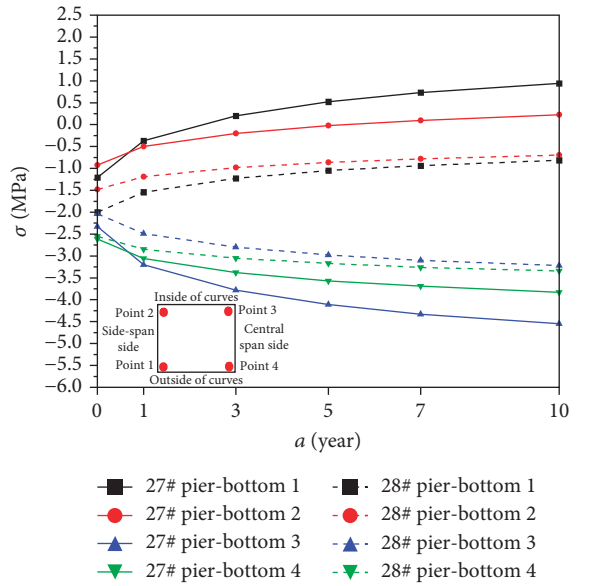

Figure 9: Main-girder concrete shrinkage and creep-induced pier-bottom normal stress.

−0.98 mm to 1.24 mm. The three types of deformation show a trend of slow increase, and the deformation of the two piers is obviously asymmetric. Therefore, in the closure jacking process of a curved PCCR bridge, it is necessary to control the longitudinal, lateral, and torsion deformations of piers.

The main-girder concrete shrinkage and creep-induced pier-bottom normal stress during bridge operation period are shown in Figure 9, where the normal stress "+" is tension and "−" is compression.

From Figure 9, it can be seen that the pier-bottom normal stress varied under the effect of concrete creep and shrinkage with the bridge operation, and the changing rate reduces gradually. In addition, the pier-bottom lateral compressive stress at the central span side increases obviously, and the pier-bottom lateral compressive stress reserve at the side span decreases gradually. Especially, the lateral stress of Pier 27# side span even transforms from compressive to tensile in three years. It can be also noticed that the changing rate of the normal stress on the outside of the curve is faster than the inside of the curve due to concrete shrinkage and creep making pier bear the transverse bending moment.

To sum up, under the action of main-girder concrete shrinkage and creep, the longitudinal displacement varies toward to the central span, and the lateral displacement varies toward to the inside of the curve. The torsional deformation will be generated at the pier-top. The pier vertical normal stress reserve of the side span will decrease, and at last the tensile stress will even appear. Therefore, it is necessary to carry out the pushing on the mid-span girder before bridge closure so as to improve the pier stress state after the bridge formed.

4.2. Closure Jacking Force Effect on Piers' Deformation. The pier-top longitudinal displacement, transverse displacement, and torsional angle may change with the CJF variation. The relationship between displacement and the CJF on the pier-top of Pier 27# and Pier 28# just after bridge completion is shown in Figure 10, where x is the displacement, θ is the torsion angle, and F is the CJF.

It can be seen from Figure 10 that with the jacking force increasing the pier-top deformation trend is opposite to that of pier caused by concrete shrinkage and creep shown in Figure 8. The pier-top longitudinal displacement, transverse displacement, and torsional angle show an obvious linear relationship with the CJF. The pier-top torsional angle and longitudinal displacement of Pier 27# change from 0.54×10^{-4} rad and 5.81 mm to -1.25×10^{-4} rad and −8.60 mm with the jacking force increasing from 0 kN to 1000 kN, respectively. The jacking force will be required about 3000 kN and 4000 kN to make them change to zero, respectively. The pier-top torsion angle and longitudinal displacement of Pier 28# change from -0.27×10^{-4} rad and −4.12 mm to 2.33×10^{-4} rad and 5.98 mm with the jacking force increasing from 0 kN to 1000 kN, respectively. The jacking force will be required about 2000 kN and 4000 kN to make them change to zero. Especially, because piers of long-span and small-radius curved PCCR bridges bear large transverse bending moment, and the curves outside prestress tendons are tensile, these make the piers bend to the outside of the curved girder. The CJF further aggravates the bending of piers. Thus, it can be observed that affected by the differences of the prestress, longitudinal, and transverse bending stiffness, and torsion stiffness of piers, the CJF of the curved PCCR bridge cannot eliminate or control the longitudinal and transverse bending and torsion of piers to reach an ideal state simultaneously. The jacking force cannot simultaneously make all the longitudinal and transverse bending and

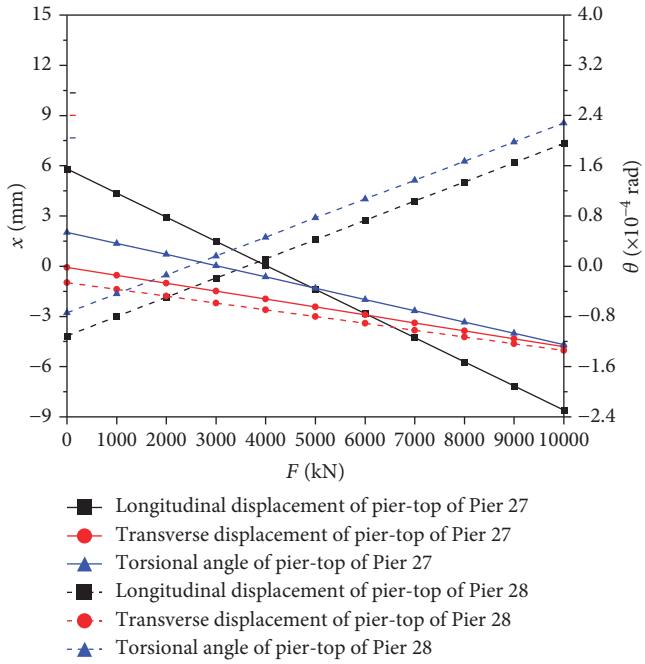

Figure 10: Relationship between pier-top displacement and the jacking force just after bridge completion.

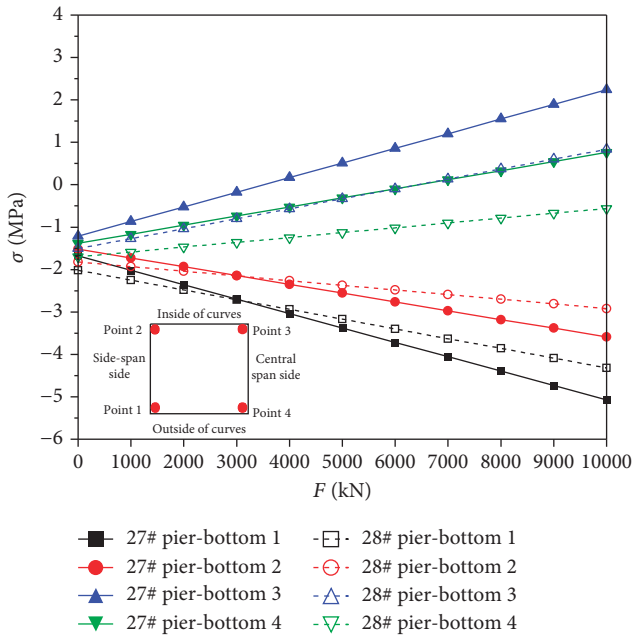

Figure 11: Relationship between the pier-bottom stress and the jacking force after jacking process.

torsional deformation of piers to be zero. This makes the CJF more difficult to determine for curved PCCR bridges.

4.3. Closure Jacking Force Effect on Piers' Normal Stress. Under the permanent load, the relationships between the piers' normal stress and the jacking force after jacking process, bridge completion, and ten years of bridge operation are shown in Figures 11 to 13, where σ is the normal stress and F is the CJF. The pier-bottom normal stress is just listed, and the tensile stress is taken as "+."

It can be seen from Figures 11 to 13 that the pier-bottom normal stress presents an obvious linear relationship with the jacking force. With the jacking force increasing, the pier-bottom pressure stress at the side span increases linearly, and the pier-bottom pressure stress at the central span side decreases linearly. The pier-bottom stress change rates inside and outside the curves are different. This is mainly because the jacking force makes the pier suffer not only longitudinal bending but also lateral bending. Therefore, for the closure jacking process of the curved PCCR bridge, both longitudinal and transverse bending of piers should be considered. Besides, the stress change of Pier 27# with small anti-pushing rigidity (with small cross-sectional area) is significantly greater than that of Pier 28# with great anti-pushing rigidity (with large cross-sectional area), and more attention should be paid to the piers' stress with smaller anti-pushing rigidity during the closure jacking process. It can be seen from Figure 13 that the pier-bottom tension stress occurs on the side span of Pier 27# after ten years of bridge operation, so the jacking force application can improve the piers' stress state. With the jacking force increasing, the tensile stress gradually decreased and will finally transform to compression. However, Figures 11 and 12 show that in the jacking process and after bridge completion, a very large jacking force causes the pier-bottom tensile stress at the central span side. Therefore, proper CJF is very crucial in controlling the piers' stress state.

4.4. Closure Jacking Force Effect on Main-Girder Normal Stress. Considering that the moment arm from the top of the thrust pier to the action line of the closure thrust is the longest and the transverse bending moment generated is also the largest, the main-girder normal stress at the cantilever root is displayed. After different closure jacking forces, the relationships between the normal stress and the closure jacking force on the cantilever root of the main-girder central span just after the jacking process, bridge completion, and ten years of operation are shown in Figures 14 to 16.

From Figures 14 to 16, it can be seen that the main-girder normal stress at the cantilever root of the central span has an obvious linear relationship with the jacking force. With the jacking force increasing, the compressive stress on the outside of the curve raises, while the compressive stress on the inside of the curve decreases. However, the closing jacking force does not transfer the normal stress from compressive to tensile, and the closing jacking force increases from 0 kN to 10000 kN while the normal stress only changes 1 MPa. The normal stress of the main-girder always has a large reserve of compressive stress. Therefore, the closure jacking force will only influence the pier stress, and insufficient and excessive jacking force will generate tensile stress only for piers. The determination of the closure jacking force should be considered that piers maintain in optimal stress state after the bridge completion.

4.5. Closure Jacking Force Calculation Results. Curved PCCR bridges suffer longitudinal and transverse bending and torsion under the action of concrete shrinkage and creep.

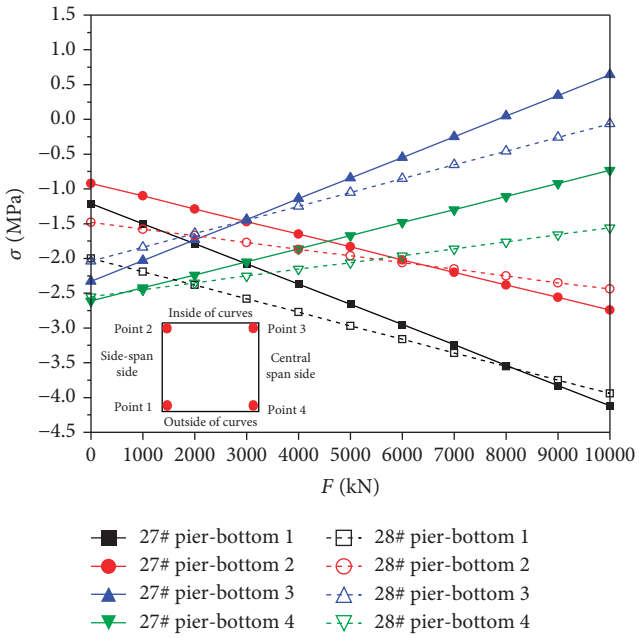

Figure 12: Relationship between the pier-bottom stress and the jacking force after bridge completion.

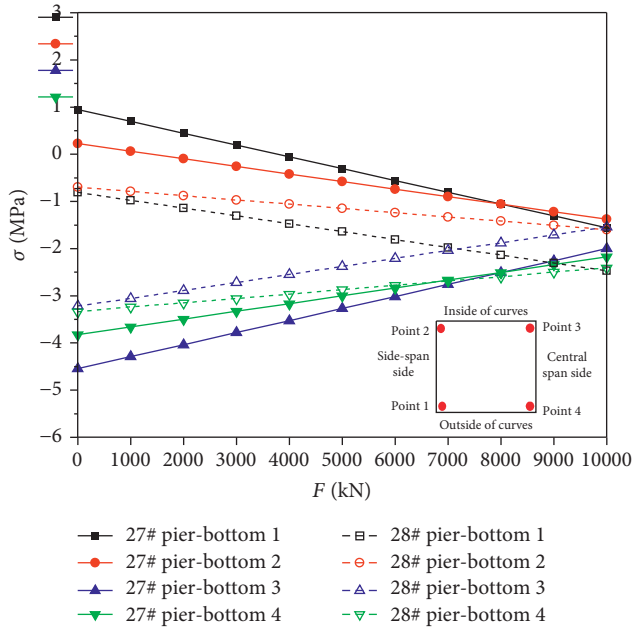

Figure 13: Relationship between the pier-bottom stress and the jacking force after ten years of bridge operation.

Although CJF can affect the longitudinal and transverse bending and torsional deformation of piers simultaneously, it cannot eliminate all deformations synchronously. Thus, the CJF and normal stress of piers show an obvious linear relationship. In addition, the closure jacking process can reduce the pier eccentricity and make the piers reach full-section compression for improving torsion stiffness [21, 22]. Therefore, in order to determine the jacking force, the effect of torque on the piers can be ignored, and it just only needs to consider the effect of jacking force on the longitudinal and transverse bending of piers. Finally, the overall stress state of piers is determined by checking the pier principal stress.

The optimal solution obtained with the multi-objective linear programming method is closely related to the objective function, but at present, there is no unified standard or theoretical basis for the control of closure jacking, and there is no unified objective. By summarizing the literature [11–17], it can be found that the concrete shrinkage and creep can be fully developed after ten years of bridge operation, and there are two main methods to determine CJF: the first method is to offset the influence of concrete shrinkage and creep for ten years after bridge completion; the second method is to offset half of concrete shrinkage and creep for ten years after bridge completion, or the effect of concrete shrinkage and creep for three years after bridge completion, or half of concrete shrinkage and creep for the thirty years after bridge completion. The core of the second method is simply to take into account the stress state of piers after bridge completion and after ten years of bridge operation. Therefore, in this study, three objectives under permanent action were selected to determine the jacking force.

(1) Objective I: the optimal stress state of piers just after bridge completion.

(2) Objective II: the optimal stress state of piers considering both that after bridge completion and ten years of bridge operation.

(3) Objective III: the optimal stress state of piers after ten years of bridge operation.

To consider the differences in the jacking effects of two piers of the PCCR bridges with asymmetric cantilever, the bottom and top of two piers were selected as control sections. Besides, to fully consider the effect of the CJF on longitudinal and transverse bending of piers, four corner points of each control section were selected as stress control points, and the corresponding objective functions were established according to the objectives I, II, and III, and with the stress at control points as the constraint condition, the multi-objective linear programming algorithm by MATLAB Optimization Toolbox was used for calculation. The initial jacking force was assumed as 7500 kN, and the optimal jacking forces of objectives I, II, and III can be obtained by several iterations with 5,332 kN, 6,975 kN, and 12,997 kN, respectively. The corresponding stress results in the state of just after bridge completion and ten years of bridge operation are shown in Table 1, and pier-top displacement results are shown in Table 2.

Tables 1 and 2 show that the optimal jacking force of a curved PCCR bridge using multi-objective linear programming method can fully reflect the influence of the longitudinal and transverse bending of piers. The jacking force significantly affects the normal stress and deformation on piers in the state of bridge completion and ten years after bridge operation, while it has relatively small effect on the maximum principal stress of piers. With the optimal stress of piers in the state of bridge completion (objective I), control points 1 and 2 at the bottom of Pier 27# have small pressure stress reserve after ten years of bridge operation under the

Table 1: Pier stress at each stage under different jacking forces (unit: MPa).

Position	Jacking force 5332 kN (objective I)		Jacking force 6975 kN (objective II)		Jacking force 12997 kN (objective III)	
	Just after bridge completion	Ten years of bridge operation	Just after bridge completion	Ten years of bridge operation	Just after bridge completion	Ten years of bridge operation
27# pier-bottom 1	−2.76	−0.39	−3.24	−0.80	−4.99	−2.31
27# pier-bottom 2	−1.89	−0.63	−2.19	−0.90	−3.29	−1.86
27# pier-bottom 3	−0.75	−3.19	−0.26	−2.77	1.53	−1.24
27# pier-bottom 4	−1.61	−2.95	−1.30	−2.68	−0.17	−1.69
27# pier-top 1	−4.64	−5.07	−4.57	−5.03	−4.33	−4.89
27# pier-top 2	−3.89	−5.10	−3.72	−4.97	−3.06	−4.51
27# pier-top 3	−1.60	−1.29	−1.65	−1.31	−1.83	−1.41
27# pier-top 4	−2.34	−1.26	−2.51	−1.37	−3.10	−1.79
27# pier	0.06*	0.57*	0.07*	0.42*	1.70*	0.06*
28# pier-bottom 1	−2.02	−2.84	−1.86	−2.69	−1.26	−2.13
28# pier-bottom 2	−0.99	−2.33	−0.66	−2.05	0.53	−1.03
28# pier-bottom 3	−1.99	−1.18	−2.15	−1.33	−2.73	−1.87
28# pier-bottom 4	−3.03	−1.70	−3.35	−1.97	−4.52	−2.97
28# pier-top 1	−0.78	−0.21	−0.89	−0.27	−1.30	−0.49
28# pier-top 2	−7.42	−7.38	−7.32	−7.28	−6.94	−6.91
28# pier-top 3	−9.83	−10.40	−9.70	−10.30	−9.25	−10.10
28# pier-top 4	−3.19	−3.22	−3.28	−3.31	−3.61	−3.64
28# pier	1.11*	0.95*	1.19*	0.96*	1.51*	1.19*

The numbers with "*" denote the maximum principal stress, and others denote vertical normal stress on each stress point of piers. With no jacking force, the maximum principal stresses for Pier 27# in the state of bridge completion and ten years after bridge operation are 0.29 MPa and 1.09 MPa, respectively; those for 28# pier are 0.97 MPa and 0.96 MPa, respectively.

Table 2: Pier-top displacement results under different jacking forces.

Pier	Item	Jacking force 5332 kN (objective I)		Jacking force 6975 kN (objective II)		Jacking force 12997 kN (objective III)	
		In the state of bridge completion	Ten years after bridge completion	In the state of bridge completion	Ten years after bridge completion	In the state of bridge completion	Ten years after bridge completion
27#	Longitudinal displacement/mm	−1.87	9.54	−4.24	7.26	−12.91	−1.11
	Transverse displacement/mm	−2.59	2.15	−3.37	1.44	−6.23	−1.13
	Torsion angle/×10-4 rad	−0.41	1.28	−0.71	0.97	−1.79	−0.17
28#	Longitudinal displacement/mm	1.97	−6.53	3.85	−4.75	10.77	1.79
	Transverse displacement/mm	−3.15	−0.57	−3.81	−1.13	−6.26	−3.18
	Torsion angle/×10-4 rad	0.87	−0.85	1.36	−0.34	3.18	1.51

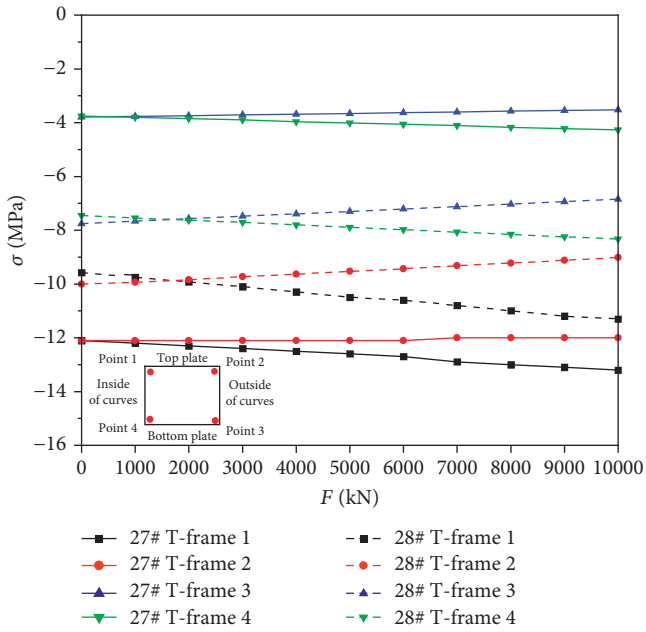

Figure 14: Relationship between the main-girder normal stress and the jacking force at central span cantilever root just after jacking process.

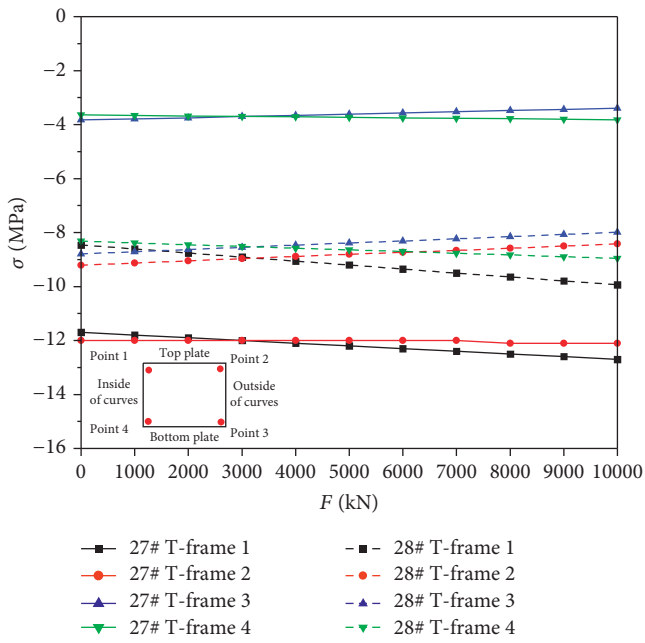

Figure 15: Relationship between the main-girder normal stress and the jacking force at central span cantilever root just after bridge completion.

action of temperature and live load, and the tensile stress is nearly to occur. After ten years of bridge operation, the pier-top has large longitudinal displacement. Taking the optimal stress of piers after ten years of bridge operation as the objective (objective III), control point 3 at the bottom of Pier 28# will have tensile stress, and a larger longitudinal displacement will occur, too. Taking the optimal stress of piers

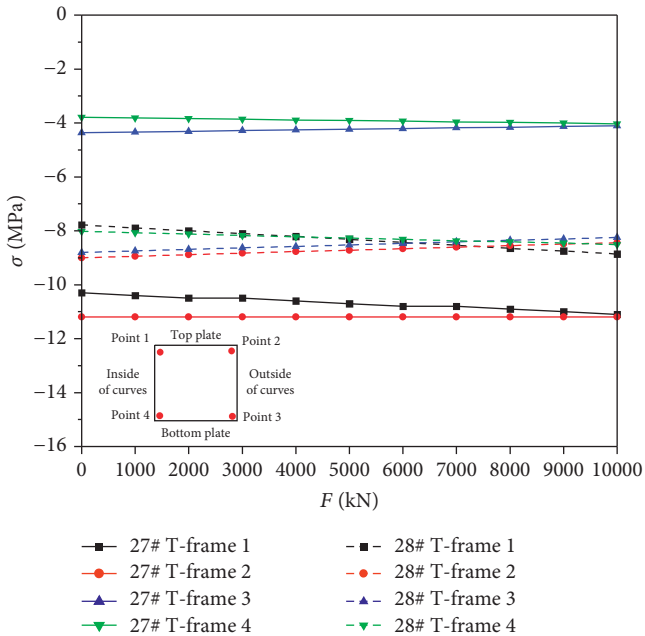

Figure 16: Relationship between the main-girder normal stress and the jacking force at central span cantilever root after ten years of bridge operation.

considering both above states (objective II) as the objective, there is no tensile stress occurrence instead of a certain reserve of compressive stress, and the displacement on pier-top is smaller. Therefore, objective II should be selected as the control objective for closure jacking force determination by considering the stress states both after bridge completion and ten years of bridge operation.

5. Conclusions

In this study, a closure jacking force calculation algorithm for curved prestressed concrete continuous rigid-frame bridges with asymmetric cantilevers and piers was proposed. Firstly, an expression for mechanical relationship between normal stress of piers and the jacking force was derived, and the effects of concrete shrinkage and creep and jacking force on deformation and stress of piers were analyzed. By clarifying that the closure jacking force and the longitudinal and transverse deformation of piers show a linear relationship, a closure jacking force calculation algorithm was proposed for solving the optimal jacking force based on the multi-objective linear programming method. The main conclusions are as follows:

(1) Under the action of concrete shrinkage and creep and the jacking force, the piers of curved continuous rigid-frame bridges may suffer longitudinal and transverse bending and torsion, and the influence of concrete shrinkage and creep and the jacking force on piers are opposite.

(2) The jacking force can also make the beam of curved continuous rigid-frame bridges produce transverse bending and torsional deformation.

(3) The jacking force significantly affects the normal stress of the one pier with a small bending stiffness, which should be paid more attention during the jacking process.

(4) The pier normal stress and the jacking force always show an obvious linear relationship in three states of jacking construction process, bridge completion, and ten years of bridge operation.

(5) The jacking force can be calculated by constrained multi-objective linear programming method, which can satisfyingly consider both the longitudinal and transverse bending of piers. When considering both the optimal stress state of bridge completion and ten years of bridge operation as the objective, no tensile stress and smaller displacement existence are produced on the pier.

Data Availability

The data are available from author Chuang Chen (email: chenchuang@nit.zju.edu.cn).

Conflicts of Interest

The authors declare no conflicts of interest.

Acknowledgments

This research was funded by the China Shanghai Railway Bureau Research Project, grant no. 2018144.

References

[1] C. B. Yin, J. J. Wang, and C. Tang, "Algorithms for the jacking force of high-temperature closure of a continuous rigid-frame bridge," *Journal of Central South University of Forestry & Technology*, vol. 1, no. 29, pp. 111–116, 2009.

[2] Y. S. Zou and R. X. Shan, "The confirmation closure jacking force of continuous rigid frame bridge," *Jouenal of Chongqing Jiaotong University*, vol. 25, no. 02, pp. 12–15, 2006.

[3] R. X. Shan and Y. H. Shan, "The confirmation of closure jacking force in continuous rigid frame bridge[J]," *Applied Mechanics and Materials*, vol. 638, pp. 987–993, 2014.

[4] C. G. Liu and C. B. Yin, "Analysis and experiment on jacking force with high temperature closure for continuous rigid frame bridge," *Highway Engineer*, vol. 34, no. 05, pp. 83–86+97, 2009.

[5] K. P. Luan, X. S. Zhang, and H. R. Gao, "Numerical method of continuous rigid frame bridge jacking force for optimization," *Ludong University Journal (Natural Science edition)*, vol. 27, no. 01, pp. 92–96, 2011.

[6] F. Zhang and Y. Wang, "Studies on closure jacking force and closure temperature of the continuous rigid frame bridge with Vshaped pier," in *Proceedings of the 2018 7th International Conference on Sustainable Energy and Environment Engineering (ICSEEE 2018)*, Atlantis Press, Shenzhen, China, November 2018.

[7] Y. Z. Jing, "Construction control of closure segment of asymmetric continuous rigid frame," *Northern Communications*, no. 12, pp. 80–83, 2012.

[8] G. Y. Tu, D. H. Yan, and K. B. Zhang, "Calculation method and countermeasure for closure temperature influence in trussed CFST arch bridge," *Engineering Mechanics*, vol. 25, no. 4, pp. 236–240, 2008.

[9] Y. Wu, R. Liu, Z. Zou et al., "Closure jacking force of multi-objective optimization of multi-span extra-dosed cable-stayed bridge," *Journal of Railway Science and Engineering*, vol. 15, no. 06, pp. 1481–1486, 2018.

[10] Z. J. Liu, "Research on design and construction of long connecting, high pier, large-span and dissymmetry continuous rigid-frame bridge," *Journal of Railway Engineering Society*, vol. 27, no. 12, pp. 31–36+46, 2010.

[11] J. Li, Y. F. Zeng, H. Chen et al., "Study on mid-span jacking force for long span continuous rigid-frame bridges," *Journal of Railway Science and Engineering*, vol. 12, no. 02, pp. 335–341, 2015.

[12] L. Qin, J. F. Chen, H. Y. Hu et al., "Study of incremental launching schemes for closure of Beipanjiang River Bridge," *World Bridges*, vol. 41, no. 03, pp. 43–46, 2013.

[13] M. L. Xu and L. J. Luo, "Control of pushing for closure of central span of Paidiao River Bridge No.1," *Bridge Construction*, no. 04, pp. 79–82, 2011.

[14] Q. J. Sun and J. Zhao, "Study of bridge closure pushing schemes based on finite element model," *Bulletin of Surveying and Mapping*, no. 08, pp. 78–81, 2015.

[15] W. S. Wen, "Construction control of continuous rigid-frame structure of auxiliary bridge of Sutong Bridge," *Bridge Construction*, no. 04, pp. 65–69, 2008.

[16] G. G. Zhang and C. N. Wu, "Discussion on jacking force design of continuous rigid frame bridg," *Journal of China & Foreign Highway*, vol. 31, no. 05, pp. 119–123, 2011.

[17] Y. Q. Liang, "Research on closure scheme and jacking force calculation of high pier and multi-span continuous rigid frame bridge," *High*, vol. 61, no. 08, pp. 116–119, 2016.

[18] L. S. Yao, *Curved Beams*, China Communications Press, Beijing, China, 1989.

[19] V. Vlasov, *Thin-walled Elastic beam*, National Science Foundation, Washington. D. C., USA, 2nd edition, 1961.

[20] X. M. Sonh, H. Melhem, L. J. Chrng et al., "Optimization of closure jacking forces in multispan concrete rigid-frame bridges," *Journal of Bridge Engineering*, vol. 22, no. 03, 2017.

[21] Y. Y. Xu, Y. He, and Q. F. Wang, "Study on the torsion performances of concrete specially shaped columns under the actions of compression bending, shear and torsion," *Engineering Mechanics*, vol. 31, no. 6, pp. 101–109, 2014.

[22] W. F. Ren and F. Li, "Research on torsion stiffness of reinforced concrete compression-flexure-shear-torsion components," *Journal of Railway Science and Engineering*, vol. 08, no. 3, pp. 42–46, 2011.